Implicit-explicit Runge-Kutta method for combustion simulation

Article · January 2006

CITATIONS
4

READS
550

6 authors, including:

Damir Valiev
Tsinghua University
57 PUBLICATIONS **1,076** CITATIONS
SEE PROFILE

Per Lötstedt
Uppsala University
129 PUBLICATIONS **3,099** CITATIONS
SEE PROFILE

Michael A. Liberman
Nordic Institute for Theoretical Physics
410 PUBLICATIONS **4,179** CITATIONS
SEE PROFILE

European Conference on Computational Fluid Dynamics
ECCOMAS CFD 2006
P. Wesseling, E. Oñate and J. Périaux (Eds)

IMPLICIT-EXPLICIT RUNGE-KUTTA METHOD FOR COMBUSTION SIMULATION

E. Lindblad[1,2], D.M. Valiev[2], B. Müller[1], J. Rantakokko[1,3], P. Lötstedt[1], M.A. Liberman[2]

[1]Department of Information Technology, Uppsala University, Box 337, 751 05 Uppsala, Sweden
e-mail: erik.lindblad@it.uu.se
web page: http://www.it.uu.se/katalog/erikl
[2]Department of Physics, Uppsala University, Box 530, 751 21 Uppsala, Sweden
e-mail: damir.valiev@fysik.uu.se
[3]UPPMAX, Uppsala University, Box 337, 751 05 Uppsala, Sweden
web page: http://www.uppmax.uu.se

Key words: Semi-implicit methods, stiff problems, combustion, deflagration-to-detonation transition

Abstract. *New high order implicit-explicit Runge-Kutta methods have been developed and implemented into a finite volume code to solve the Navier-Stokes equations for reacting gas mixtures. The resulting nonlinear systems in each stage are solved by Newton's method. If only the chemistry is treated implicitly, the linear systems in each Newton iteration are simple and solved directly. If in addition certain convection or diffusion terms are treated implicitly as well, the sparse linear systems in each Newton iteration are solved by preconditioned GMRES. Numerical simulations of deflagration-to-detonation transition (DDT) show the potential of the new time integration for computaional combustion.*

1 INTRODUCTION

The distinctive feature of premixed combustion is its ability to propagate as a self-sustained wave of the exothermic chemical reaction spreading through a homogeneous combustible mixture either as a subsonic deflagration (premixed flame) or supersonic detonation. Thus, both deflagration and detonation appear to be stable attractors each being linked to its own base of initial data.

In unconfined obstacle-free systems the concrete realization of the specific propagation mode is controlled by the ignition conditions. Normally, deflagrations are initiated by a mild energy discharge, i.e. by a spark, while detonations are provoked by shock waves via localized explosions. It is known, however, that in the presence of obstacles or confinement (tube walls, wire screens, porous matrix, etc.) the initially formed deflagration undergoes gradual acceleration abruptly converting into detonation [1, 2, 3, 4, 5]. In spite

of numerous efforts, the basic mechanisms controlling the spontaneous transition from deflagrative to detonative combustion (DDT) is still remaining a major unsolved challenge of the combustion theory [6, 7, 8, 9].

The classical explanation of DDT [1, 2, 3] was due to flame acceleration in a tube caused by the flame interaction with the nonuniform flow ahead of the flame front, which is formed by the flame pushing the unburned gas in a tube with adhesive walls. The nonuniform flow stretches the flame, so that the shape of the flame mimics the velocity profile in the flow ahead. This increases the flame surface area, thus accelerating the reaction wave propagation and the flow. This flame-acceleration phenomenon is presumably enhanced by the flame interaction with turbulence generated in the boundary layer formed in the flow ahead of the flame [1, 2, 10]. Indeed, it has recently been realized [11] that the hydraulic resistance alone is capable of triggering the transition even if the multi-dimensional effects, such as the flame acceleration due to folding, are completely suppressed and the system is regarded as effectively one-dimensional. The basic predictions of the one-dimensional model were recently corroborated by direct numerical simulations of premixed gas combustion in thin channels, where the hydraulic resistance is incorporated through the no-slip boundary condition rather than through the volumetric drag-force [12]. It was also recently shown [13, 14] that a similar effect is observed in wide channels and in the channels with rough walls. For both no-slip and rough walls the transition is triggered predominantly by hydraulic resistance inducing formation of an extended preheat zone ahead of the advancing flame, and thereby creating conditions pertinent to Zeldovich's mechanism of soft initiation. The detonation first develops in the near-wall mixture adjacent to the flame, corroborating many experimental observations (e.g. [7]).

Deflagration-to-detonation transition in unconfined systems is more problematic. There are reports claiming that in highly sensitive oxygen-based mixtures the transition may be triggered by outwardly propagating 'free-space' flames [15]. In this description, the transition is commonly attributed to the flame acceleration induced by the Darrieus-Landau (DL) instability (spontaneous flame wrinkling). Yet, the acceleration resulting from the wrinkling seems to be a rather weak effect whose ability to cause the transition is not at all obvious. In the foreword to Nettleton's monograph on gaseous detonation [3], when discussing the problem of transition, Zel'dovich wrote, "The role of the internal instability of the plane slow flame (Landau, Darrieus) is still not clear."

As is now well known, (e.g. [16, 17, 18, 19, 20, 21]) in wide channels the DL instability results in the formation of wrinkled flames and the flame speed enhancement due to the increase of the flame area. The wrinkled flame generates a shock with a Mach number of about 1.2 - 1.5, which is too low to trigger detonation. Yet, as has recently been shown [13, 14, 22, 23], there is another previously overlooked aspect of the DL instability. The folded reaction zone creates a low-gradient preheating (preconditioning) of the fresh mixture trapped within the fold interior. This, under favorable conditions, may invoke autoignition triggering the transition. The mechanism of the transition is the temperature increase

due to the influx of heat from the folded reaction zone, followed by autoignition. The transition occurs when the pressure elevation at the accelerating reaction front becomes high enough to produce a shock capable of supporting detonation. This requires the fold to be sufficiently narrow and deep. The effect was found to be sensitive to the flame's normal speed and the reaction rate pressure-dependency, favoring fast flames and high-order reactions. In the context of colliding elliptic flames the folding induced transition was reported also in [24] and for flame initiated by corrugated walls in [25].

A central issue in simulations of combustion is to ensure that the computations resolve all the most important flow and chemical time and space scales. To simulate combustion processes from first principles, it is necessary to resolve the relevant scales from the size of the system to the flame thickness, a range that can cover up to twelve orders of magnitude. This computational challenge in the development of numerical algorithms for solving coupled partial and ordinary differential equations resulted in the development of several numerical methods, including adaptive mesh refinement to deal with multiscale phenomena, domain decomposition, and multiresolution methods using wavelets.

The present work is aimed at gaining further improvement of the numerical code performance for modeling complex combustion processes. The present simulations were performed using a parallel version of the code developed by L.-E. Eriksson [26]. This code solves the Navier-Stokes equations for reacting gas mixtures using a third-order upwind-biased finite volume method for the inviscid fluxes and a second-order central discretization of the viscous fluxes with an explicit second order Runge-Kutta time integration method. The code has been successfully used for solving physics problems of flame instability in wide tubes [16, 18, 20] and gaining deeper understanding of DDT in wide tubes with thermoisolated (adiabatic boundary conditions) and rough walls [13, 14, 22, 23]. Further steps in the DDT studies will include investigation of heat losses to the walls, influence of complex chemistry and flame-turbulence interaction, and simulations in 3D. These additions increase the stiffness of the governing equations and therefore the time stepping method must be improved.

In the present study, new time integration methods have been implemented into the combustion code, namely second and fourth order implicit-explicit Runge-Kutta methods [28] [29], as well as a third order implicit-explicit Runge-Kutta method [36]. Whereas the inviscid and viscous fluxes are treated explictly, the chemistry is treated implicitly. Since only the species continuity equations have nonzero chemistry terms, the resulting nonlinear systems only involve the species densities and are quickly solved by Newton's method. Other classifications of non-stiff and stiff parts of the equations have been investigated as well. Then, the resulting nonlinear systems are solved using efficient Jacobian matrix calculations and GMRES. The systems are preconditioned using incomplete LU factorizations. Preliminary results show that the increased stability of the implicit method combined with the efficiency of the explicit method will be an efficient solver for the intended combustion problems.

2 NAVIER-STOKES EQUATIONS FOR REACTING GAS

2.1 Thermodynamic, Transport and Chemical Models

We consider a thermally perfect gas mixture of n species M_i with the molecular weights W_i and the densities ρ_i. The mass fraction of species i (meaning M_i) is the ratio of the mass of species i and the mass of the mixture, i.e.

$$Y_i \;=\; \frac{\rho_i}{\rho}, \tag{1}$$

where ρ is the density of the mixture. Details of the thermodynamic model we used are given by Kuo [30].

Viscosity, molecular diffusion and heat conduction are described by simplified transport models. For the viscosity μ, we use the Sutherland law. The Schmidt numbers

$$Sc_i \;=\; \frac{\mu}{\rho D_i} \tag{2}$$

of all species are assumed to be equal and constant. D_i denotes the diffusion coefficient of species M_i and is determined from equation (2) by the specified Schmidt number and the computed density and viscosity. The Prandtl number

$$Pr \;=\; \frac{c_p \mu}{\kappa} \tag{3}$$

is assumed to be constant. c_p and κ are the specific heat at constant pressure and the heat conduction coefficient of the mixture, respectively.

We consider a chemical reaction mechanism with m reactions [30]. A reaction h (here h is an index for reactions and not the enthalpy) is of the form

$$\sum_{k=1}^{n} \nu'_{k,h} M_k \longrightarrow \sum_{k=1}^{n} \nu''_{k,h} M_k, \tag{4}$$

where $\nu'_{k,h}$ and $\nu''_{k,h}$ are the stoichiometric coefficients of reaction h for species k appearing as a reactant and as a product, respectively. The reaction rate of reaction h is

$$k_h \prod_{k=1}^{n} \left(\frac{\rho_k}{W_k} \right)^{\nu'_{k,h}} \tag{5}$$

with W_k the molecular weight of species k and the Arrhenius term

$$k_h = A_h T^{\alpha_h} exp\left(\frac{-E_h^a}{R_u T} \right), \tag{6}$$

where A_h and α_h are constants and E_h^a is the activation energy of reaction h. R_u is the universal gas constant, and T is the temperature. The backward reaction of reaction (5) is

$$\left(\frac{k_h}{K_h^C}\right) \prod_{k=1}^{n} \left(\frac{\rho_k}{W_k}\right)^{\nu''_{k,h}}. \tag{7}$$

The equilibrium constants

$$K_h^C = \prod_{k=1}^{n} \left(\frac{\rho_k}{W_k}\right)^{(\nu''_{k,h}-\nu'_{k,h})}_{equilibrium} \tag{8}$$

are functions of temperature, and tables exist for most of them [31]. With the definitions above, the production rate ω_i of species i is given by

$$\omega_i = W_i \sum_{h=1}^{m} (\nu''_{i,h} - \nu'_{i,h}) k_h \left(\prod_{k=1}^{n} \left(\frac{\rho_k}{W_k}\right)^{\nu'_{k,h}} - \frac{1}{K_h^C} \prod_{k=1}^{n} \left(\frac{\rho_k}{W_k}\right)^{\nu''_{k,h}} \right). \tag{9}$$

2.2 Navier-Stokes equations

In Cartesian coordinates, the 2D compressible Navier-Stokes equations for reacting gas flow read in conservative form [30, 17]

$$\frac{\partial \mathbf{U}}{\partial t} + \frac{\partial (\mathbf{F} - \mathbf{F}_v)}{\partial x} + \frac{\partial (\mathbf{G} - \mathbf{G}_v)}{\partial y} = \mathbf{S}, \tag{10}$$

where $\mathbf{U}$ is the vector of the conservative variables, $\mathbf{F} = \mathbf{F}_1$ and $\mathbf{G} = \mathbf{F}_2$ are the inviscid flux vectors for the x- and y-directions, and $\mathbf{F}_v = \mathbf{F}_{v1}$ and $\mathbf{G_v} = \mathbf{F}_{v2}$ are the viscous flux vectors for the x- and y-directions. Let the Cartesian coordinates and velocity components be denoted by $(x_1, x_2)^T = (x, y)^T$ and $(u_1, u_2)^T = (u, v)^T$. The pressure, the total energy per unit mass, the total enthalpy, and the enthalpy of species k are denoted by p, E, H, and h_k, respectively. Then the conservative variables, the inviscid and viscous flux vectors are

$$\mathbf{U} = \begin{pmatrix} \rho \\ \rho u_1 \\ \rho u_2 \\ \rho E \\ \rho Y_1 \\ \vdots \\ \rho Y_{n-1} \end{pmatrix}, \mathbf{F}_j = \begin{pmatrix} \rho u_j \\ \rho u_1 u_j + p\delta_{1j} \\ \rho u_2 u_j + p\delta_{2j} \\ \rho H u_j \\ \rho_1 u_j \\ \vdots \\ \rho_{n-1} u_j \end{pmatrix}, \mathbf{F}_{vj} = \begin{pmatrix} 0 \\ \tau_{1j} \\ \tau_{2j} \\ \sum_{l=1}^{2} u_l \tau_{lj} + \kappa \frac{\partial T}{\partial x_j} + \rho \sum_{k=1}^{n} \left(D_k h_k \frac{\partial Y_k}{\partial x_j} \right) \\ D_1 \rho \frac{\partial Y_1}{\partial x_j} \\ \vdots \\ D_{n-1} \rho \frac{\partial Y_{n-1}}{\partial x_j} \end{pmatrix} \tag{11}$$

and $\mathbf{S}$ is the source term

$$\mathbf{S}^T = (0, 0, 0, 0, \omega_1, \ldots, \omega_{n-1}) .$$

For a Newtonian fluid, the components of the shear stress tensor are

$$\tau_{ij} = \mu \left(\frac{\partial u_i}{\partial x_j} + \frac{\partial u_j}{\partial x_i} \right) - \frac{2}{3} \mu \left(\sum_{k=1}^{2} \frac{\partial u_k}{\partial x_k} \right) \delta_{ij}$$

where $\delta_{ij} = 1$ if $i = j$ and $\delta_{ij} = 0$ if $i \neq j$.

Integrating equation (10) over a control volume Ω (actually a surface in 2D) with the boundary $\partial\Omega$ and the outer normal unit vector $\mathbf{n} = (n_x, n_y)^T$ and using the Gauss theorem, we obtain the integral form of the 2D Navier-Stokes equations for a reacting gas flow

$$\int_\Omega \frac{\partial \mathbf{U}}{\partial t} dV + \int_{\partial\Omega} (\mathbf{F} - \mathbf{F}_v) n_x dA + \int_{\partial\Omega} (\mathbf{G} - \mathbf{G}_v) n_y dA = \int_\Omega \mathbf{S} dV. \tag{12}$$

3 FINITE VOLUME METHOD

With the finite volume method, equation (12) is discretized for each grid cell by approximating

$$\frac{d\mathbf{U}_{i,j}}{dt} Vol_{i,j} + \sum_{s=1}^{N} [(\mathbf{F} - \mathbf{F}_v) n_x A + (\mathbf{G} - \mathbf{G}_v) n_y A]_s = \mathbf{S}_{i,j} Vol_{i,j}. \tag{13}$$

where $\mathbf{U}_{i,j}$ is the volume averaged vector of the conservative variables in the cell $\Omega_{i,j}$ and $\mathbf{S}_{i,j}$ the volume averaged source vector. $Vol_{i,j}$ is the area of the cell. Since we consider structured grids with quadrilaterals as control volumes, the cells have $N = 4$ sides. A_s is the length of the cell interface s. The cell averages $\mathbf{U}_{i,j}$ are the unknowns in the cell-centered finite volume method. Therefore, we have to approximate the flux vectors at the cell interfaces. The inviscid flux vectors are discretized by a third-order upwind-biased approximation of the characteristic variables and using a total variation diminishing (TVD) limiter [26] [27]. Central discretizations are employed for the viscous fluxes at the cell interfaces. The volume averaged nonlinear source term is approximated by

$$\mathbf{S}_{i,j} \approx \mathbf{S}(\mathbf{U}_{i,j}). \tag{14}$$

After the finite volume discretization of equation (13), we have a system of ordinary differential equations (ODEs) for the time dependent cell averages $\mathbf{U}_{i,j}$

$$y' = f(y) + g(y) , \tag{15}$$

where y denotes the vector of all $\mathbf{U}_{i,j}$, $f(y)$ the vector of all inviscid and viscous flux contributions, i.e. all $-\frac{1}{Vol_{i,j}} \sum_{s=1}^{N} [(\mathbf{F}^n - \mathbf{F}_v^n) n_x A + (\mathbf{G}^n - \mathbf{G}_v^n) n_y A]_s$, and $g(y)$ the vector

of all source terms $\mathbf{S}_{i,j}$. Thereby, we classify the right hand side of the ODE (15) into a non-stiff part f and a stiff part g. Other classifications are possible and discussed in section 6.2.

4 IMPLICIT-EXPLICIT RUNGE-KUTTA METHODS

We have developed high order implicit-explicit Runge-Kutta (IERK) methods to efficiently solve separable stiff problems (15) [28, 29]. While first-order IERK methods have frequently been used to treat the stiff source terms from chemistry implicitly in hypersonic flow and combustion simulations [32, 33], two of our new IERK methods are second order accurate and one is fourth order accurate. Similar high order IERK methods have only recently been available [34, 35, 36, 37, 38].

An explicit Runge-Kutta (ERK) method is used to solve the non-stiff part f and a diagonally implicit Runge-Kutta (DIRK) method is employed to solve the stiff part g. A general s-stage implicit-explicit Runge-Kutta (IERK) method consists of an s-stage ERK and an s-stage DIRK method with common weighting coefficients $b_i, i = 1, ..., s$. The following tableaus define the ERK and DIRK methods of an IERK method [28, 29]:

$$\begin{array}{c|cccc} 0 & & & \\ \varepsilon_{21} & 0 & & \\ | & & 0 & \\ \varepsilon_{s1} & - & \varepsilon_{s,s-1} & 0 \\ \hline b_1 & - & - & b_s \end{array} \qquad \begin{array}{c|cccc} a_{11} & & & \\ a_{21} & a_{22} & & \\ | & & & \\ a_{s1} & - & - & a_{ss} \\ \hline b_1 & - & - & b_s \end{array} \tag{16}$$

The approximate solution y^{n+1} at $t = (n+1)\Delta t$ is defined by

$$\begin{aligned} &y^{n+1} = y^n + \Delta t \sum_{i=1}^{s} b_i k_i \ , \text{ where} \\ &k_i = f\left(y^n + \Delta t \sum_{j=1}^{i-1} \varepsilon_{ij} k_j\right) + g\left(y^n + \Delta t \sum_{j=1}^{i} a_{ij} k_j\right), \\ &i = 1, \ldots, s. \end{aligned} \tag{17}$$

The coefficients of our 4th order accurate 5-stage IERK method denoted as IERK45 method are given in Table 1.

5 PARALLELIZATION

The original code is parallelized using the Message Passing Interface (MPI). Since the solver is designed to handle multi-block grids the processors are first divided into clusters, one cluster for each sub-block. The number of processors in each cluster are chosen to optimize the load balance using the clustering algorithm in [39]. The blocks are then partitioned in two dimensions within the corresponding processor cluster. Almost all calculations can be performed locally within the processors except for the flux calculations which require data from its nearest neighbors. The exchange of data is handled with out-of-order non-blocking communication using MPI's persistent communication objects.

Table 1: Coefficients for fourth order implicit-explicit Runge-Kutta method IERK45

$\epsilon_{21} = 0.39098372452428$	$a_{11} = 1/4$
$\epsilon_{31} = 1.09436646160460$	$a_{21} = 0.34114705729739$
$\epsilon_{32} = 0.33181504274704$	$a_{22} = 1/4$
$\epsilon_{41} = 0.14631668003312$	$a_{31} = 0.80458720789763$
$\epsilon_{42} = 0.69488738277516$	$a_{32} = -0.07095262154540$
$\epsilon_{43} = 0.46893381306619$	$a_{33} = 1/4$
$\epsilon_{51} = -1.33389883143642$	$a_{41} = -0.52932607329103$
$\epsilon_{52} = 2.90509214801204$	$a_{42} = 1.15137638494253$
$\epsilon_{53} = -1.06511748457024$	$a_{43} = -0.80248263237803$
$\epsilon_{54} = 0.27210900509137$	$a_{44} = 1/4$
$b_1 = a_{51}$	$a_{51} = 0.11933093090075$
$b_2 = a_{52}$	$a_{52} = 0.55125531344927$
$b_3 = a_{53}$	$a_{53} = -0.1216872844994$
$b_4 = a_{54}$	$a_{54} = 0.20110104014943$
$b_5 = a_{55}$	$a_{55} = 1/4$

The solver has been tested on a Sun Fire 15k server with UltraSparcIIIcu processors running at 900MHz. The largest partition of the machine has 36 processors and 36GB RAM. Each processor has 64KB L1-cache and 8MB L2-cache. We have run several test cases with different problem sizes (600x200 to 1000x200 grid points) and different numbers of blocks (1 to 5 blocks in the multi-block case). All cases show excellent scaling with superlinear speedup up to full machine size, i.e., speedup close to 40 on 36 processors, cf. Figure 1 [40]. The superlinear speedup is due to better cache utilization as data is divided into smaller pieces when running on multiple processors.

6 RESULTS

6.1 Deflagration to Detonation Transition (DDT)

One of the typical pictures of the transition due to formation of the appropriate flame fold is shown in Fig. 2, where the sequence of zonal images depicting the square of pressure gradient gives a cinematic impression of the dynamics of the flame front during the incipient stage of the transition from deflagration to detonation [14]. These images resemble the schlieren photographs of laboratory experiments, though the latter visualize gradients of the density rather than of the pressure.

The numerical resolution is 10 cells per flame width. The time instants of Fig. 2 are not evenly spaced but rather clustered around the transition point. The earlier images depicting the incipient phase of the flame evolution in the vicinity of the tube's closed end, are not shown.

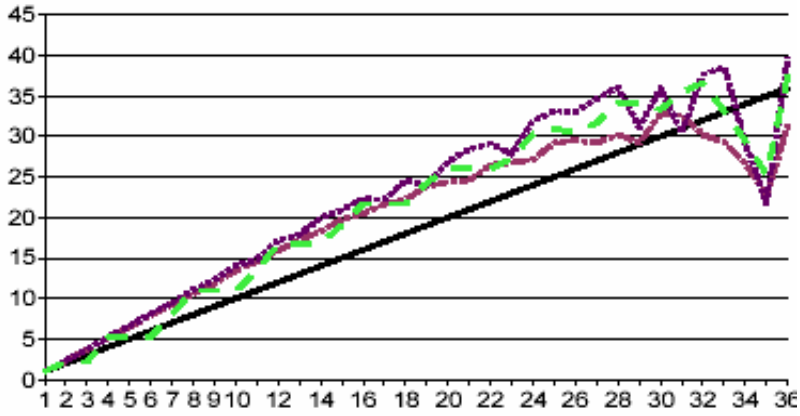

Figure 1: Speedup versus number of processors for 3 blocks running on a SunFire 15k, − ideal speedup, .−. 1D decomposition of each block separately, ... 2D decomposition of each block separately, −− dividing the processors among the blocks [40]

A zoomed view of the flame fold dynamics near the transition point is shown in Fig. 3 [14]. The associated profiles of temperature, density, flow velocity, and pressure along the fold axis are plotted on Fig. 4 [14]. Here one readily observes (i) formation of the large-scale preheat zone (preconditioning) in the unreacted gas trapped within the fold interior, (ii) acceleration of the fold-tip, and (iii) the pressure elevation and formation of a high pressure peak. The transition occurs when the pressure peak becomes high enough to produce a shock capable of supporting detonation. This requires the fold to be narrow and deep enough; otherwise one ends up with a moderately strong pressure wave insufficient for triggering the transition. This mechanism of transition by an appropriate non-uniformity in the temperature field (preconditioning) may naturally be associated with Zel'dovich's theory of soft initiation [41, 42].

6.2 Test of IERK Methods

To show the advantages of using IERK methods for combustion a series of DDT simulations have been performed. The flux is calculated using the combustion code of [26]. The original code uses a second order explicit Runge-Kutta method known as Gary's method [43] for the time stepping. For our tests it has been replaced by implicit-explicit Runge-Kutta methods of order 2, 3 and 4. The third order method is derived in [36], and the second and fourth order methods are derived in [28, 29]. Simulations showing order of accuracy and applications of IERK methods to various model problems are also presented in the cited source papers.

6.2.1 Static implicit treatment of chemistry

As stated above the code by [26] has been successfully used for combustion calculations. The need for implicit treatment of the chemistry becomes evident when studying the transition from deflagration to detonation for a propagating flame. Fig. 5 shows the temperature contours of the DDT simulation obtained using the original explicit code. Soon after the transition the solution becomes unstable.

Since the chemical source term (14) only depends on cell data, the implicit iteration can be performed by solving a $(3+n)\times(3+n)$ system per cell where n is the number of species. In the present simulations a mixture of two species representing burned and unburned fuel is used. The production rate of the fuel is given by an Arrhenius expression, cf. (9) and (6).

$$\omega_1 = -A\rho^{m-1}\rho Y exp\left(\frac{-E^a}{R_u T}\right), \tag{18}$$

where Y is the mass fraction of the fuel, A the reaction rate constant, and E^a the activation energy. Here m denotes the reaction order. The temperature T is dependent on ρY and given by

$$T = \frac{E - H_0 - \frac{1}{2}\left(u^2+v^2\right)}{C_v} \tag{19}$$

where E is the total energy per unit mass, ρ is the density and u and v are velocities in x and y directions, respectively. The enthalpy of formation H_0 and the specific heat at constant volume C_v for a mixture of n species are given by

$$H_0 = \sum_{i=1}^{n} Y_i H_{0_i} \tag{20}$$

$$C_v = \sum_{i=1}^{n} Y_i C_{v_i} \tag{21}$$

H_{0_i} and C_{v_i} are corresponding values for species i. For the present case $n=2$, $C_{v_1} = C_{v_2}$ and $H_{0_2} = 0$ and (19) thus reduces to

$$T = \frac{E - Y H_{0_1} - \frac{1}{2}\left(u^2+v^2\right)}{C_{v_1}} \tag{22}$$

This reduces the implicit treatment of the source term (18) to a scalar equation which can be solved using scalar Newton iteration without having to solve any linear systems or compute Jacobians. The overhead for solving the chemistry implicitly is therefore very small. Fig. 6 shows the temperature contours obtained for the same setup as the explicit case above but using the first order implicit Euler method for the chemistry treatment. Here the solution remains stable during the transition.

The DDT for the implicit-explicit code occurs after roughly twice the time as for the explicit code. This is because of the chaotic behaviour of the perturbations on the flame front that cause the cusps and thereby trigger the DDT. Therefore direct comparisons cannot be made between the two cases, but the main observation is that the explicit code becomes unstable shortly after the DDT when choosing the time step based on the stability conditions for the inviscid and viscous parts.

6.2.2 Flexible treatment of flux terms using "switch" technique

Although the implicit treatment of the chemistry term proves efficient to retain stability during DDT, apart from being more efficient than fully implicit methods, the real benefits come from being able to configure the explicit and implicit treatment more flexibly. Consider an ODE or a semi-discretized PDE consisting of several separable terms:

$$U'(t) = \sum_{i=1}^{l} F_i\left(t, U\right) \ . \tag{23}$$

For a given problem some of the F_i terms will be non-stiff and some will be stiff. Every F_i will yield an upper limit on the time step for an explicit method to remain stable, the stiffer the term the smaller the limiting time step. When using an explicit method the most restrictive time step will be used for all F_i terms, resulting in unnecessary evaluations of the other terms. When the stiffness varies significantly among the F_i terms the use of IERK methods can be more efficient than fully explicit or implicit methods, as shown above.

The stiffness can vary in the course of a simulation, both in time and space. For combustion simulations the flux gradients are steepest near the flame, which moves continuously. Depending on the specific problem cell shapes, grid configurations and boundary layer effects greatly affect which F_i term will yield the most restrictvie time step.

For these situations it is beneficial to be able to freely choose which F_i terms are treated implicitly. In the Navier-Stokes example the F_i consists of three terms, inviscid flux, viscous flux and chemical source term. In the next example, a flame propagating in a tube similar to the case described above, the limiting time step for the inviscid and viscous fluxes are calculated in each step, the chemical source term is always treated implicitly. For this problem the viscous terms yield a more than 100 times smaller limiting time step than the inviscid terms. This small step size is not needed to maintain accuracy and therefore we choose to treat also the viscous terms implicitly. This enables us to use a time step limited only by the inviscid terms.

To investigate the impact of a larger time step a reference solution is computed explicitly using a time step $\Delta t_{ref} = 4 \cdot 10^{-11}$ s, calculated from the stability condition of the viscous terms. This is compared with the solutions obtained when using a time step $\Delta t_{IERK} = 4 \cdot 10^{-9}$ and treating the viscous terms and chemistry implicitly.

The nonlinear equations in each stage of the IERK methods are solved by Newton's method. The Jacobian matrices are calculated by a variant of TOMS 618 [44]. The linear systems in each Newton iteration are solved by the generalized minimum residual method (GMRES) with a restart vector length of 20. Krylov methods like GMRES are well suited for solving large, sparse linear systems [45, 46, 47]. The implementation used is from [48]. To increase the convergence rate of the GMRES iterations preconditioning is used. Several types of incomplete LU-factorizations (ILU) have been tested and the simulations discussed here use ILU0 preconditioning from SPARSKIT [49, 50]. The ILU0 preconditioning is a very simple technique where no new non-zero elements are introduced during the ILU factorization, thereby allowing for efficient storage of the sparse matrices.

Fig. 7 shows the density contours at $t = 1000\Delta t_{ref}$, $t = 5000\Delta t_{ref}$ and $t = 10000\Delta t_{ref}$. The results obtained with IERK45 are in good agreement with those obtained with the explicit second order Runge-Kutta method (ERK2). Although the computational work per time level is larger, IERK45 is more efficient than ERK2, because the time step for IERK45 can be chosen 100 times larger than for ERK2.

The original code is set to recalculate the grid as the wave propagates. The grid update is dependent on the current solution and therefore direct comparisons of the solutions would be misleading. The differences in the final solutions would originate both from the solution interpolation and from the longer time step and a direct comparison would not be possible. Therefore a fixed grid was used to obtain the results shown in figure 7.

6.2.3 Dynamical configuration of explicit and implicit treatment

A general approach to deal with the varying stiffness in time and space is to use adaptive mesh refinement, AMR, to concentrate the grid resolution on areas where it is needed. To give even more efficiency the configuration of which F_i terms are treated explicitly and which are treated implicitly can be changed dynamically during a simulation. The same mechanisms for deciding when to refine or coarsen the grid resolution can be used to switch implicit treatment of different terms on and off. In this way the expensive implicit solvers are only used where absolutely needed.

7 CONCLUSIONS

A new time discretization has been developed for integration of the equations of combustion. By treating parts of the unknown variables implicitly and the remaining parts explicitly in a Runge-Kutta method, significant savings in computing time are possible. The chemistry equations in each cell are advanced by an implicit time-stepping in one example. The time step restrictions in an explicit method due to the stiffness in the chemistry model are then avoided. In another model example, the viscous and chemistry terms are integrated implicitly and compared to explicit integration for all components. The resulting CFL number with the implicit-explicit method is up to 100 times larger than with the explicit scheme without hampering the accuracy in the solution.

ACKNOWLEDGEMENTS

Fellowships for E. Lindblad by EU and Göran Gustafsson Foundation are gratefully acknowledged by M. Liberman and B. Müller, respectively.

REFERENCES

[1] Schelkin, K. I. and Troshin, Ya. K., *Gasdynamics of Combustion*, Mono Book Corp. Baltimore, 1965.

[2] Zel'dovich, Ya. B., Kompaneets, A.S., *Theory of Detonation*, Academic press, New York, 1960.

[3] Nettleton, M. A., *Gaseous Detonation*, Chapman and Hall, London, 1987.

[4] Urtiew, P., and Oppenheim, A. K., Experimental observation of the transition to detonation in an explosive gas, *Proc. Roy. Soc. Lond. Ser. A*, **295**, 13-28. (1966).

[5] Oppenheim, K. and Soloukhin, R. I., Experiments in gasdynamics of explosion, *Ann. Rev. Fluid Mech.* **5**, 31-58 (1973).

[6] Lee, J.H.S. and Moen, I., The mechanism of transition from deflagration to detonation in vapor cloud explosion, *Prog. Energy Combust. Sci.*, **6**, 359-389 (1980).

[7] Shepherd, J. E., and Lee, J. H. S., *On the transition from deflagration to detonation, in Major Research Topics in Combustion*, (M. Y. Hussaini, A. Kumar, and R. G. Voigt, eds), Springer-Verlag, New York, 439-487, 1992.

[8] Buckmaster, J., Clavin, P., Linan, A.,Matalon, M., Peters, N., Sivashinsky, G., Williams, F. A., *Some developments in Combustion Theory*, Proc. Combust. Inst., 30, 1-14, (2005).

[9] Sivashinsky, G. I., *Some developments in premixed combustion modeling*, Proc. Combust. Inst., 29, 1737 (2002).

[10] Kuznetsov, M., Alekseev, V., Matsukov, I., and Dorofeev, S., DDT in a smooth tube filled with a hydrogen-oxygen mixture, *Shock Waves*, **14**, 205-215 (2005).

[11] Brailovsky, I., and Sivashinsky, G. I., Hydraulic Resistance as a Mechanism for Deflagration-to-Detonation Transition, *Combust. Flame*, **122**, 492-499 (2000).

[12] Kagan, L., and Sivashinsky, G., The transition from deflagration to detonation in thin channels, *Combust. Flame*, **134**, 389-397 (2003).

[13] Liberman, M. A., Sivashinsky, G. I., Valiev, D. M. and Eriksson, L-E., *Hydrodynamic Instability as a Mechanism for Deflagration-to-Detonation Transition*, 20th International Colloquium on the Dynamics of Explosions and Reactive Systems (ICDERS), Montreal, 2005.

[14] Liberman, M. A., Sivashinsky, G. I., Valiev, D. M. and Eriksson, L-E., Numerical Simulation of Deflagration-to-Detonation Transition: The Role of Hydrodynamic Flame Instability, *Int. J. Transport Phenomena* (2006) to appear.

[15] Sokolik, A. S. Self-Ignition, *Flame and Detonation in Gases, Israel Program for Scientific Translations*, NASA TTF-125OTS-63-1179, Jerusalem, 1963.

[16] Liberman, M. A., Golberg, S. M., Bychkov, V. V., and Eriksson, L.-E., Numerical studies of hydrodynamically unstable flame propagation in 2D channels, *Combust. Sci. Tech.*, **136**, 221-242 (1998).

[17] Bychkov, V. V. and Liberman, M. A., Dynamics and stability of premixed flames, *Physics Reports*, **325**, 115-237 (2000).

[18] Travnikov, O.Yu., Bychkov, V.V. and Liberman, M.A., Influence of compressibility on propagation of curved flames, *Physics of Fluids*, **11**, 2657-2666 (1999).

[19] Kazakov, K. A. and Liberman, M. A., Nonlinear equation for curved stationary flames, *Physics of Fluids*, **14**, 1166-1180 (2002).

[20] Liberman, M. A., Ivanov, M. F., Peil, O. E., Valiev, D. M., and Eriksson, L.-E., Numerical modeling of flame propagation in wide tube, *Combust. Theory Modeling*, **7**, 653-676 (2003).

[21] Kadowaki, S. and Hasegawa, T., Numerical simulation of dynamics of premixed flames: flame instability and vortex-flame dynamics, *Progr. Energy Combust. Sci.*, **31**, 193-241 (2005).

[22] Liberman, M. A., Sivashinsky, G. I., Valiev, D. M., *Numerical Simulation of Deflagration-to-Detonation Transition: The Role of Hydrodynamic Flame Instability*, ECCOMAS Thematic Conference on Computational Combustion, Lisbon, Portugal, (2005).

[23] Liberman, M. A., Sivashinsky, G. I., Valiev, D. M. and Eriksson, L-E., The Darrieus-Landau Instability as a Mechanism for Deflagration-to-Detonation Transition *Combust. Theory and Modeling* (2006) to appear.

[24] Oran, E. S., and Gamezo, V. N., *Flame acceleration and detonation transition in narrow tubes*, Proc. 20th ICDERS, Montreal, Canada (CD) (2005).

[25] Kagan L. LibermanM. Sivashinsky G, *Detonation initiation by hot corrugated walls*, ECCOMAS Thematic Conference on Computational Combustion, Lisbon, Portugal, 21-(2005).

[26] Eriksson, L.-E., *Development and validation of highly modular flow solver versions in G2DFLOW and G3DFLOW series for compressible viscous reacting flow*, Tech. Report, 9970-1162, Volvo Aero Corporation, Trollhättan, Sweden, 1995.

[27] Andersson, N., Eriksson, L.-E. and Davidson, L., Large-Eddy Simulation of subsonic turbulent jets and their radiated sound. *AIAA Journal*, **43**(9), 1899–1912, (2005).

[28] Lindblad, E., *High order semi-implicit Runge-Kutta methods for separable stiff problems*, Master's Thesis, Uppsala University, Sweden, Dec. 2004.

[29] Lindblad, E. and Müller, B., High order implicit-explicit Runge-Kutta methods for separable stiff problems. Submitted to *BIT*, Aug. 2005.

[30] Kuo, K.K., *Principles of Combustion*. John Wiley & Sons, New York, 1986.

[31] Kee, R.J., Rupley, F.M. and Miller, J.A., *CHEMKIN-II: A Fortran chemical kinetics package for the analysis of gas-phase chemical kinetics*. SANDIA Report, SAND89-8009B, 1991.

[32] Bussing, T.R.A. and Murman, E.M., Finite-volume methods for the calculation of compressible chemically reactive flows. *AIAA J.*, **26** (9), 1070–1078, (1988).

[33] Eriksson, L.-E., *Time-marching Euler and Navier-Stokes solution for nozzle flows with finite rate chemistry*. Tech. Report, 9370-794, Volvo Flygmotor AB, Trollhättan, Sweden, 1993.

[34] Ascher, U.M., Ruuth, S.J. and Spiteri, R.J., Implict-explicit Runge-Kutta methods for time-dependent partial differential equations, *Appl. Numer. Math.*, **25**, 151–167, (1997).

[35] Pareschi, L. and Russo, G., Implicit-explicit Runge-Kutta schemes and applications to hyperbolic systems with relaxation, *J. Scientific Comp.*, **25** (1/2), 129–155, (2005).

[36] Yoh, J.J. and Zhong, X., New hybrid Runge-Kutta methods for unsteady reactive flow simulation, *AIAA J.*, **42** (8), 1593–1600, (2004).

[37] Yoh, J.J. and Zhong, X., New hybrid Runge-Kutta methods for unsteady reactive flow simulation: Applications, *AIAA J.*, **42** (8), 1601–1611, (2004).

[38] Kennedy, C.A. and Carpenter, M.H., Additive Runge-Kutta schemes for convection-diffusion-reaction equations, *Appl. Numer. Math.*, **44**, 139–181, (2003).

[39] Rantakokko, J., Partitioning Strategies for Structured Multiblock Grids, *Parallel Computing*, **26** (12), 1661-1680, (2000).

[40] Myklebust, E., *Parallelization of a combustion code*, Master's Thesis, Uppsala University, Sweden, July 2004.

[41] Zel'dovich, Ya.B., Librovich, V. B., Makhviladze, G. M., and Sivashinsky, G. I., On the development of detonation in non-uniformly preheated gas *Astronautica Acta*, **15**, 313-321, (1970).

[42] Zel'dovich, Ya.B., Regime classification of an exothermic reaction with nonuniform initial conditions, *Combust. Flame*, **39**, 211-226, (1980).

[43] Gary, J., On certain finite difference schemes for hyperbolic systems, *Math. Comp.*, **18**, 1–18, (1964).

[44] Coleman, T.F., Garbow, B.S. and Moré, J.J., Algorithm 618: FORTRAN subroutines for estimating sparse Jacobian Matrices, *ACM Transaction on Mathematical Software*, **10** (3), 346-347, (1984).

[45] Knoll, D.A. and Keyes, D.E., Jacobian-free Newton-Krylov methods: a survey of approaches and applications, *J. Comput. Phys.*, **193**, 357-397, (2004).

[46] Banas, K., A Newton-Krylov solver with multiplicative Schwarz preconditioning for finite element compressible flow simulations, *Commun. Numer. Meth. Engng.*, **18**, 269-275, (2002).

[47] Pernice, M. and Tocci, M.D., A multigrid-preconditioned Newton-Krylov method for the incompressible Navier-Stokes equations, *SIAM J. Sci. Comput.*, **23** (2), 398-418, (2001).

[48] Frayssé, V., Giraud, L., Gratton, S. and Langou, J., *A set of GMRES routines for real and complex arithmetics on high performance computers*, CERFACS Technical Report TR/PA/03/0, 2003, public domain software available on `www.cerfacs/fr/algor/Softs`.

[49] Saad, Y., *SPARSKIT: a basic tool kit for sparse matrix computations (version 2)*, Report, 1994, public domain software available on `www-users.cs.umn.edu/~saad/software/SPARSKIT/sparskit.html`.

[50] Saad, Y., *Iterative Methods for Sparse Linear Systems*, 2nd ed., SIAM, Philadelphia, 2003.

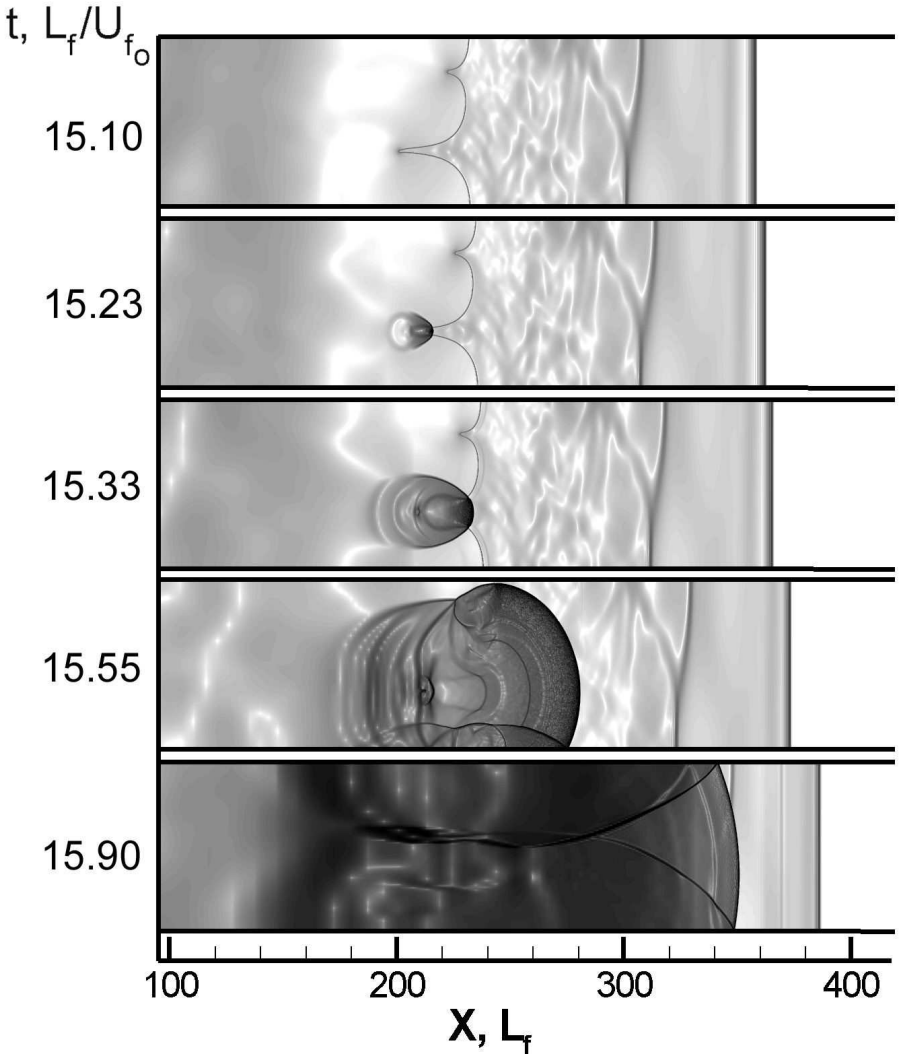

Figure 2: Time sequence of images for the flame/shock dynamics near the transition point. Stronger shading corresponds to higher pressure gradient. The time and distance are referred to L_f/U_{f_0} and L_f respectively. $L_f = \mu_u/(Pr\rho_u U_{f_0})$ is the flame width, where U_{f_0} is the incipient velocity of the planar flame, ρ_u and μ_u the density and dynamic viscosity, respectively, of the unburnt fuel. The incipient velocity of the planar flame U_{f_0} corresponds to the Mach number $M_{f_0} = U_{f_0}/c_u = 0.05$, where c_u is the speed of sound in the unburnt fuel. Reaction order $m = 2$, tube width $D = 70L_f$, dimensionless activation energy $\epsilon = E^a/(R_u T_b) = 8$, expansion ratio $\Theta = T_b/T_u = 10$. T_u and T_b are the temperatures of the unburnt and burnt gases, respectively.

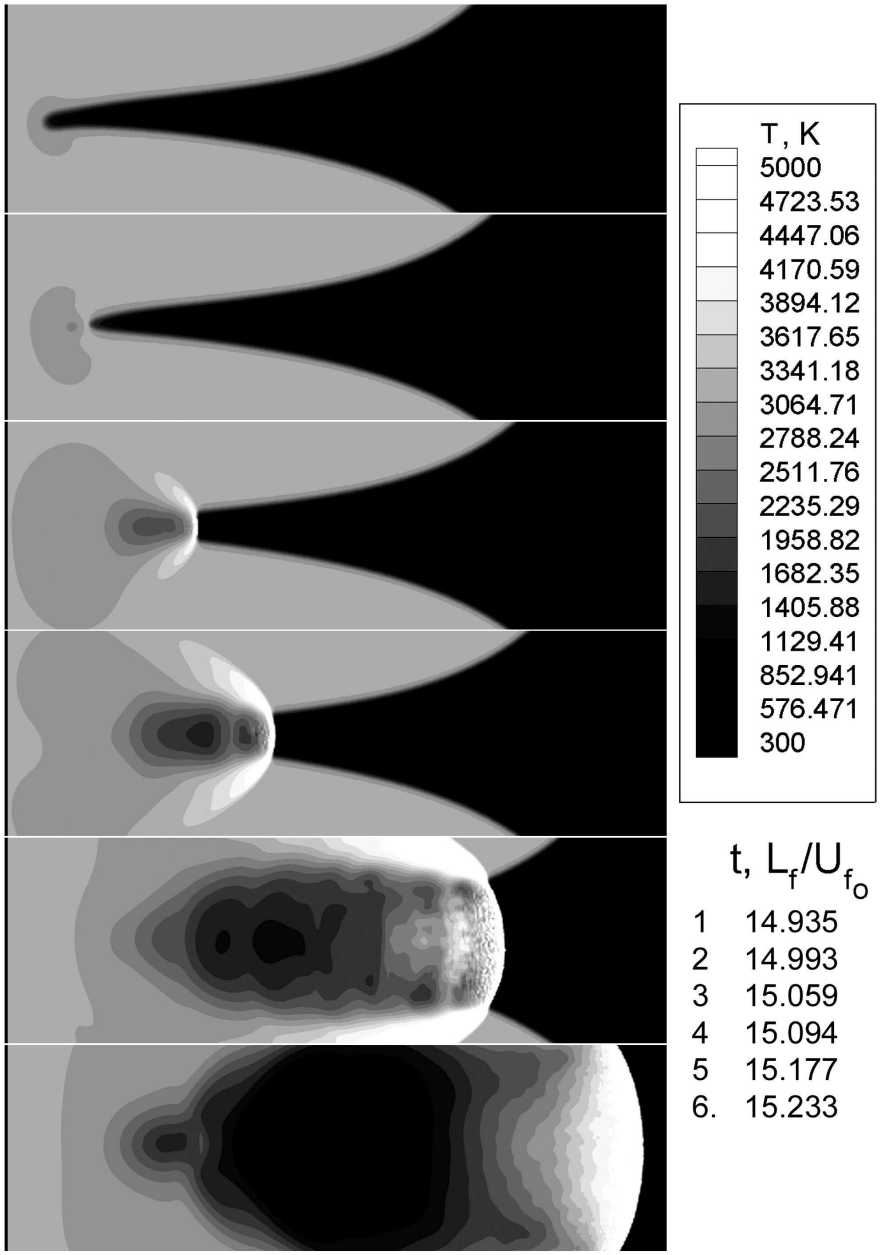

Figure 3: Time sequence of zoomed temperature contours for the flame dynamics near the transition point for the conditions of Fig. 2. Lighter shading corresponds to higher temperature.

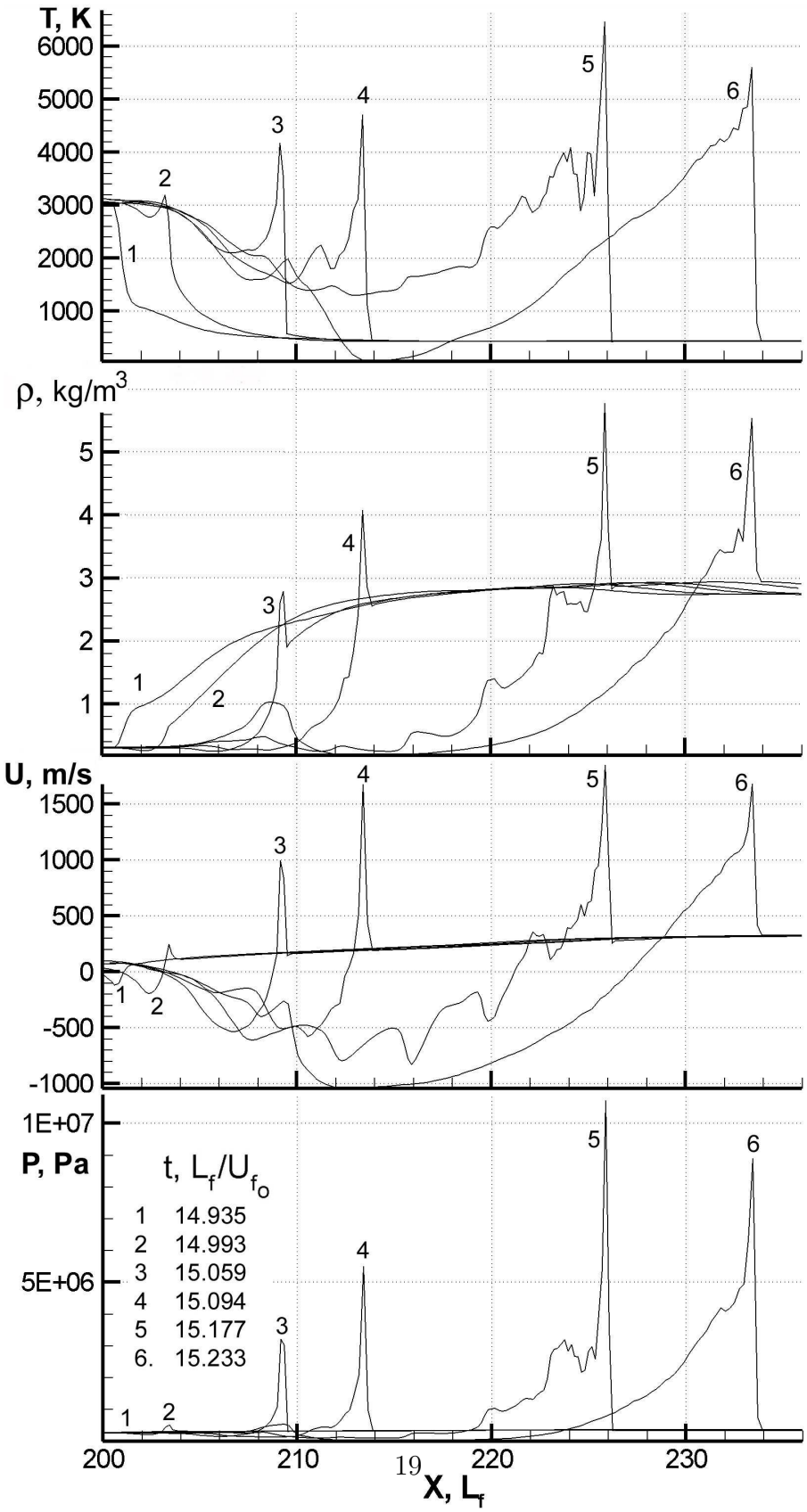

Figure 4: Temperature, density, flow velocity and pressure profiles for the fold dynamics of Fig. 3.

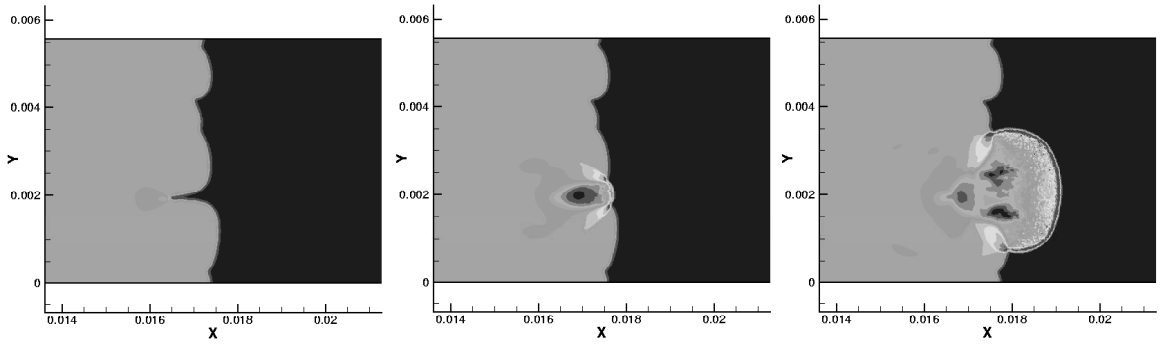

Figure 5: Temperature contours with explicit chemistry treatment which yields an earlier DDT, but cannot handle the detonation correctly and becomes unstable shortly after the last state in the series above.

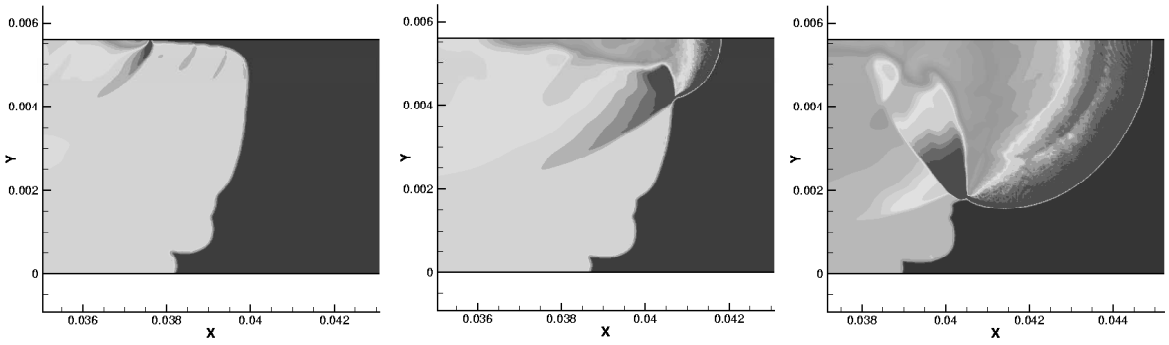

Figure 6: Temperature contours with implicit chemistry treatment. When using the implicit Euler method for chemistry, the DDT evolves with retained stability.

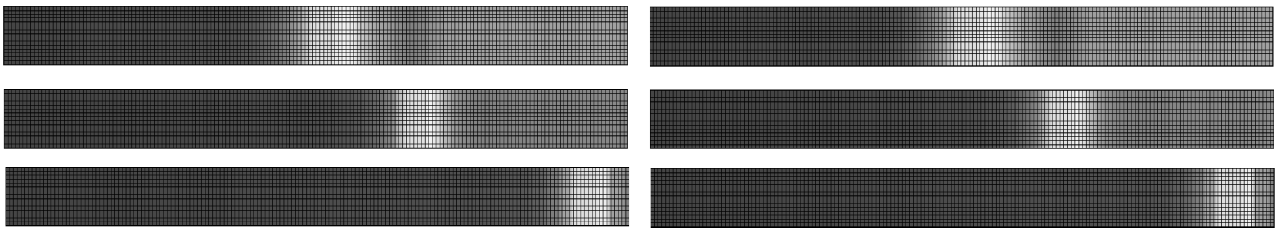

Figure 7: Density contours at $t = 1000\Delta t_{ref}$, $t = 5000\Delta t_{ref}$ and $t = 10000\Delta t_{ref}$. The reference explicit calculation is shown on the left and an implicit-explicit solution on the right. Inviscid terms are treated explicitly while viscous terms and chemistry are treated implicitly.